

## Dissociative photodetachment dynamics of the iodide-aniline cluster

M. Shane Bowen

*Department of Chemistry and Biochemistry, University of California San Diego, 9500 Gilman Drive, La Jolla, California 92093-0340*

Maurizio Becucci

*Dipartimento di Chimica, Via N. Carrara 1, Università di Firenze, Polo Scientifico dell'Università, 50019 Sesto Fiorentino (Firenze), Italy European Laboratory for Non-Linear Spectroscopy (LENS), Via N. Carrara 1, Università di Firenze, Polo Scientifico dell'Università, 50019 Sesto Fiorentino (Firenze), Italy*

Robert E. Continetti<sup>a)</sup>

*Department of Chemistry and Biochemistry, University of California San Diego, 9500 Gilman Drive, La Jolla, California 92093-0340*

(Received 22 March 2006; accepted 10 May 2006; published online 3 October 2006)

The photodetachment dynamics of the iodide-aniline cluster,  $I^-(C_6H_5NH_2)$ , were investigated using photoelectron-photofragment coincidence spectroscopy at several photon energies between 3.60 and 4.82 eV in concert with density functional theory calculations. Direct photodetachment from the solvated  $I^-$  chromophore and a wavelength-independent autodetachment process were observed. Autodetachment is attributed to a charge-transfer-to-solvent reaction in which incipient continuum electrons photodetached from  $I^-$  are temporarily captured by the nascent neutral iodine-aniline cluster configured in the anion geometry. Subsequent dissociation of the neutral cluster removes the stabilization, leading to autodetachment of the excess electron. The dependence of the dissociative photodetachment (DPD) and autodetachment dynamics on the final spin-orbit electronic state of the iodine fragment is characterized. The dissociation dynamics of the neutral fragments correlated with autodetached electrons were found to be identical to the DPD dynamics of the I atom product spin-orbit state closest to threshold at a given photon energy, lending support to the proposed sequential mechanism. © 2006 American Institute of Physics. [DOI: 10.1063/1.2210010]

### INTRODUCTION

The photodetachment dynamics of solvated halogen anions has been an active area of research yielding information about weakly interacting atoms and molecules.<sup>1-4</sup> As molecules aggregate through van der Waals forces and hydrogen bonding, solvents having polarizable unsaturated bonds such as aromatic rings exhibit a number of significant interactions, including ion-dipole, ion-quadrupole, and ion-induced polarization.<sup>5,6</sup> In the present study, the dissociative photodetachment (DPD) dynamics of the iodide-aniline cluster,  $I^-(C_6H_5NH_2)$ , are investigated using photoelectron-photofragment coincidence (PPC) spectroscopy at photon energies from 3.60 to 4.82 eV. This study focuses on the autodetachment and direct photodetachment processes this cluster anion exhibits as a result of the halide-aniline interaction.

Recently, the DPD dynamics of a series of solvated iodide clusters were investigated using PPC spectroscopy at a photon energy of 4.82 eV.<sup>7</sup> In that study, the  $I^-(C_6H_5NH_2)$  cluster was observed to exhibit solvent-induced effects in both the photodetachment dynamics of the perturbed  $I^-$  chromophore as well as the dissociation dynamics of the nascent neutral complex. The half-collision dynamics of the neutral

cluster, when configured in the equilibrium geometry of the anionic cluster, were found to be dependent on the spin-orbit state of the iodine atom at that photon energy. The photoelectron spectrum also exhibited a near-threshold electron detachment process distinct from the  $I(^2P_{3/2})$ ,  $I(^2P_{1/2})$  direct photodetachment transitions expected from the  $I^-$  constituent.<sup>1,8,9</sup>

The aniline molecule is larger than solvents previously studied by similar techniques.<sup>9-14</sup> It is a polar molecule that can interact with a halide in a number of ways. Bonding in the  $I^-(C_6H_5NH_2)$  cluster is dominated by hydrogen bonding, ion-dipole, and ion-induced-dipole forces. Even in the neutral  $I(C_6H_5NH_2)$  cluster, significant interactions between the polar aniline and polarizable I atom occur, particularly when configured in the geometry of the anion. The interactions in both the anionic and neutral complexes may have a significant impact on the photodetachment dynamics and subsequent dissociation of the neutral complex.

The near-threshold feature observed in the photoelectron spectrum of  $I^-(C_6H_5NH_2)$  at 4.82 eV suggests that an autodetaching excited anionic state is produced by photoexcitation at this energy.<sup>7</sup> Autodetachment of an electron from a stable negative ion with a range of kinetic energies can occur by an exchange of energy between the molecular core and the excess electron if the total internal energy of the anion exceeds the electron affinity.<sup>15,16</sup> The  $I^-(C_6H_5NH_2)$  cluster is not a stable anion after absorption of a 4.82 eV photon, how-

<sup>a)</sup>Author to whom correspondence should be addressed. Electronic mail: rcontinetti@ucsd.edu

ever, so an excited anionic state in the photodetachment continuum must exist. This excited state is likely to be either a charge-transfer-to-solvent (CTTS) state or a short-lived excited state arising from direct photoexcitation of the aniline moiety with subsequent energy transfer leading to autodetachment of the electron localized on  $I^-$ . The CTTS state may result from either a temporary dipole-bound state arising from the interaction of the nascent continuum electron with the dipole of the neutral complex, or charge transfer of the electron from  $I^-$  into an excited valence state of aniline.

A number of studies have examined the role of dipole-bound excited states in cluster anions. Johnson and co-workers have found evidence for these states below the threshold for photodetachment in binary clusters of iodide with polar species such as  $I^-(CH_3CN)$  and  $I^-(CH_3COCH_3)$ .<sup>12,17</sup> Dipole-bound states arise from the interaction of the electron with the permanent dipole moment of the molecule or complex. Including the effect of rotational motion, it has been predicted that long-lived dipole-bound states require a dipole moment  $\mu \geq 2$  D.<sup>18,19,21</sup> Charge-transfer studies of Rydberg atoms and polar molecules by Desfrancois *et al.*<sup>20</sup> have experimentally confirmed the production of dipole-bound states with polar molecules with  $\mu \geq 2.66$  D. Electron scattering experiments have shown that resonances supported by the dipolar field persist in systems with dipoles as small as  $\sim 1.1$  D.<sup>22,23</sup>

Johnson and co-workers have also examined the nature of the CTTS transition in  $I^-$ -water clusters, and showed that a precursor to the CTTS transition is found above the detachment threshold in clusters as small as  $I^-(H_2O)_2$ .<sup>24</sup> Given the importance of understanding the solvated electron, a number of theoretical and experimental studies have focused on the behavior of larger clusters.<sup>1,25</sup> Time-resolved photodetachment studies of the  $I^-(H_2O)_4$  cluster by Neumark and co-workers<sup>26,27</sup> have shown that a CTTS transition occurs, with vibrational autodetachment occurring from the water network in less than 200 fs. The dipole moment of the water network in that anionic cluster is enhanced to a value of 4.4 D due to the interaction with the halide relative to a vanishing dipole moment of the neutral  $(H_2O)_4$  cluster.<sup>24,28,29</sup> Szpunar *et al.* have recently studied the dissociation dynamics of the  $I(H_2O)_n$ ,  $n=2,5$ , clusters photoexcited to the CTTS band, and concluded that dissociation probably occurs after autodetachment of the excess electron, consistent with the time-resolved studies.<sup>30</sup>

The dipole moment of isolated aniline is small,  $\mu_{C_6H_5NH_2} = 1.13$  D,<sup>31</sup> and therefore dipole-bound  $C_6H_5NH_2^-$  does not exist as a stable anion. The aniline molecule has a closed shell electronic configuration and no stable valence-state molecular anion. Electron transmission measurements indicate an electron affinity (EA) for aniline of  $-1.13$  eV, with the extra electron being temporarily captured into the  $a_2(\pi_1^*)$  orbital as a short-lived ( $\tau \leq 10^{-14}$  s) anion.<sup>32</sup> However, this state may be stabilized in the anionic cluster and charge transfer to the valence excited state of aniline is a possibility. This type of behavior was observed by Cyr *et al.* in a study of photoinduced intracluster dissociative attachment in the  $I^-(CH_3I)$  complex.<sup>33</sup> Changes in the geometry and electronic properties of the molecule induced by external

factors (i.e., complex formation or interaction with a lattice) may play a critical role in the stabilization of an excess electron in either a dipole-bound or valence state.

The present studies have been undertaken to examine the origin of the autodetachment feature previously observed at 257 nm (4.82 eV). With the exception of this autodetachment feature, the previous study of  $I^-(C_6H_5NH_2)$  indicated that the extra electron in this cluster primarily remains localized on the halogen atom, with the measured vertical detachment energy (VDE) characteristic of a stabilized iodide ion and a spin-orbit electronic state separation energy the same as that of the isolated atom.<sup>7</sup> PPC measurements at several photon energies from 4.82 eV down to 3.60 eV have now been carried out, and evidence for autodetachment found at each photon energy. Following a brief review of the experimental technique, these results are presented and discussed in terms of a CTTS process leading to a transient dipole-bound anion that autodetaches upon reorganization and dissociation of the nascent neutral cluster. These coincidence measurements allow correlation of the autodetachment process with the dissociation dynamics of the nascent neutral cluster, providing further evidence for a sequential DPD process.

## EXPERIMENT

These experiments were carried out using a fast-ion-beam PPC spectrometer. The apparatus has been described in detail elsewhere,<sup>7,34,35</sup> and the specific application of the technique to examining the branching between DPD and the production of stable neutral clusters is discussed in some detail in Ref. 7, so only a brief review is now given. This experimental technique allows measurement of photoelectron energy and angular distributions in coincidence with the photofragment energy and angular distributions as well as a separation of stable versus DPD processes. In the experiments reported here, PPC images and spectra from photodetachment of  $I^-(C_6H_5NH_2)$  correlated with both bound and dissociating neutral clusters are presented.

The basic experimental technique is as follows. A fast, mass-selected beam of  $I^-(C_6H_5NH_2)$  interacts with a pulsed laser in a photoelectron spectrometer that allows recording the three-dimensional velocity of a photodetached electron.<sup>35,36</sup> The photoelectron data can be examined as either a two-dimensional image or a more conventional photoelectron kinetic energy (eKE) or photoelectron binding energy ( $eBE = E_{h\nu} - eKE$ ) spectrum. In the present experiments examination of low energy photoelectrons is useful so the photoelectron spectra are presented as both  $v_z$ -sliced  $N(eKE)$  spectra that are very sensitive to the presence of low eKE photoelectrons and also as detector-acceptance-function-corrected  $P(eKE)$  spectra, representing the full Franck-Condon intensity distribution recovered from the higher-resolution  $v_z$ -sliced  $N(eKE)$  spectra.<sup>37</sup> Residual anions are deflected out of the beam and any neutrals, either stable clusters or  $I + C_6H_5NH_2$  photofragments, are then detected in coincidence with a time- and position-sensitive detector, yielding product translational energy spectra,  $N(E_T)$ . The

coincidence measurement permits the separation of photodetachment events yielding stable clusters from DPD processes.

The primary difference in the experimental technique used in the present work compared with that in Ref. 7 is that tunable radiation generated by an optical parametric amplifier (OPA) (Light Conversion TOPAS-4/400) pumped by the second harmonic of a regeneratively amplified Ti:sapphire laser [Clark CPA 2000,  $\sim 1.8$  ps full width at half maximum (FWHM)] was used to study the wavelength dependence of the DPD of  $I^-(C_6H_5NH_2)$ . The OPA was used to generate 310 nm (4.00 eV), 330 nm (3.76 eV), and 344 nm (3.60 eV) radiations, with power densities of  $\approx 20$ –60 MW/cm<sup>2</sup>. These results are compared with earlier experiments using the third harmonic, 257 nm (4.82 eV,  $\approx 120$  MW/cm<sup>2</sup>), of the same laser. All wavelengths were monitored using an Ocean-Optics spectrometer (USB-2000) as well as by performing calibration measurements on  $I^-$  at each photon energy.

## QUANTUM CHEMISTRY CALCULATIONS

In order to gain insights into the  $I^-(C_6H_5NH_2)$  and  $I(C_6H_5NH_2)$  clusters, quantum chemical calculations were performed using the GAUSSIAN 2003 program suite.<sup>38</sup> The equilibrium geometries, frequencies of the vibrational modes, electric dipole moments, and energetics of the  $I^-(C_6H_5NH_2)$  cluster, the associated neutral cluster, and its constituents were calculated using density functional theory (DFT). These calculations were performed using the B3LYP hybrid exchange correlation functional with a different basis set for the iodine and aniline constituents for computational feasibility as in previous studies.<sup>39,40</sup> The iodine atom was described using the GAUSSIAN 03 DGDZVP basis set<sup>41</sup> and aniline was described using the aug-cc-pVDZ basis set,<sup>42</sup> providing for inclusion of polarization and diffuse functions. The stabilization energy of the clusters with respect to the fragments was calculated taking into account the basis set superposition error (BSSE) using the counterpoise method.<sup>43</sup>

The geometry optimizations were performed without symmetry constraints and a wide range of different starting conformations was sampled in the search for a global minimum. Series of initial geometries for both the anionic and neutral clusters were probed with the iodine atom configured to initially interact with the  $\pi$  electrons in the aromatic ring, the H atom on the phenyl group opposite to the N atom, the H atoms on the side of the phenyl group, and the H atoms on the amino group. All optimizations were found to converge to the minimum energy structures presented here. The optimized equilibrium structures of  $I^-(C_6H_5NH_2)$  and  $I(C_6H_5NH_2)$  are shown in Fig. 1 and reported in Table I. The energetics and other properties for the clusters, as well as the neutral cluster fixed in the geometry of the anionic cluster, are given in Table II, along with results for isolated aniline, I and  $I^-$ . The single-point calculations of the neutral cluster fixed in the anion geometry yield the VDE of the anionic cluster and the electric dipole moment of the nascent  $I(C_6H_5NH_2)$  cluster formed in the geometry of  $I^-(C_6H_5NH_2)$ .

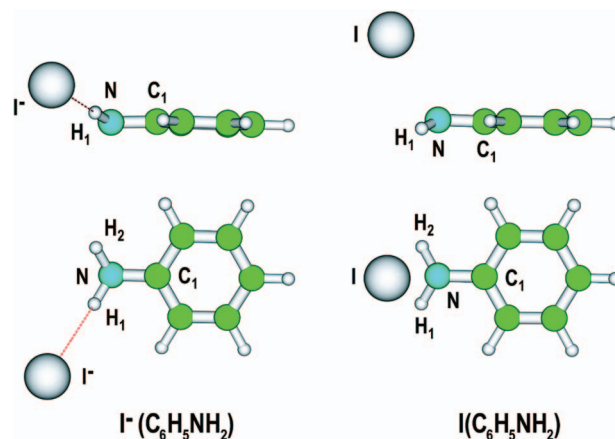


FIG. 1. (Color) Illustrations of the DFT optimized geometries of the iodine-aniline anionic (left) and neutral (right) clusters. Atom labels used for identification of interatomic distances and angles in Table I and within the text are shown.

The calculations on the  $I^-(C_6H_5NH_2)$  cluster predict a hydrogen bonding interaction between one of the amino hydrogens and  $I^-$ , while the  $I(C_6H_5NH_2)$  cluster is predicted to have a minimum energy configuration with the I atom interacting primarily with the lone-pair electrons on the N atom. These structures are related through inversion of the pyramidal geometry around the N atom in aniline and I atom translation. It was not possible to find a local minimum for the neutral cluster in a conformation similar to this anionic geometry. The interaction of  $I^-$  with aniline distorts the aniline fragment relative to the isolated molecule. In particular, the N–H<sub>i</sub> bond lengths are predicted to be longer and the N–C<sub>1</sub> bond length is predicted to be shorter in the anionic cluster. The calculations indicate that conjugation between the lone-pair electrons on the nitrogen atom and the aromatic ring results in the decreased N–C<sub>1</sub> bond length in the anion complex. In the neutral cluster, all three of these bond lengths are seen to approach the values observed for the isolated molecule.<sup>44</sup> The DFT calculations of the neutral cluster when configured in the optimized geometry of the anionic cluster predict that the electric dipole moment of the neutral cluster

TABLE I. DFT geometries for iodine-aniline anionic and neutral clusters. [calculated at the B3LYP/DGDZVP level for iodine atom and the B3LYP/aug-cc-pVDZ level for aniline using the direct inversion in the iterative subspace option (gdiis) (Ref. 51) and “very tight” convergence criteria]. Bond lengths are in Å and angles are in degrees.

Anion coordinate	Distance/angle	Neutral coordinate	Distance/angle
I–H <sub>1</sub>	2.697	I–N	2.926
I–N	3.718	I–H <sub>1</sub>	3.077
I–H <sub>2</sub>	4.139	I–H <sub>2</sub>	3.077
I–C <sub>1</sub>	4.608	I–C <sub>1</sub>	3.840
N–H <sub>1</sub>	1.027	N–H <sub>1</sub>	1.011
N–H <sub>2</sub>	1.010	N–H <sub>2</sub>	1.011
N–C <sub>1</sub>	1.378	N–C <sub>1</sub>	1.392
$\angle I-H_1-N$	172.632	$\angle C_1-NI$	121.420
$\angle I-NC_1$	122.499	$\angle C_1-NH_1$	118.280
$\angle H_1-NH_2$	113.011	$\angle C_1-NH_2$	118.280
$\angle C_1-NH_1$	118.642	$\angle H_1-NH_2$	114.181
$\angle C_1-NH_2$	116.773	$\angle INH_{1(2)}$	88.851

TABLE II. Summary of DFT calculations (calculated at the B3LYP/DGDZVP level for iodine and B3LYP/aug-cc-pVDZ level for aniline) and experimental results for the  $\Gamma^-(\text{C}_6\text{H}_5\text{NH}_2)$ ,  $\text{I}(\text{C}_6\text{H}_5\text{NH}_2)$ , and  $\text{C}_6\text{H}_5\text{NH}_2$  species. Energies are stated in Hartrees unless otherwise noted; BSSE is the counterpoise-corrected basis set superposition error, VDE is the vertical detachment energy, EA is the adiabatic electron affinity, and  $|\mu|$  is the magnitude of the electric dipole moment. Asterisks ( \*) indicate single-point energy and dipole calculations of the neutral cluster and aniline fragment when frozen in the optimized geometry of the anion.

System	$\Gamma^-(\text{C}_6\text{H}_5\text{NH}_2)$	$\text{I}(\text{C}_6\text{H}_5\text{NH}_2)^*$	$(\text{C}_6\text{H}_5\text{NH}_2)^*$	$\text{I}(\text{C}_6\text{H}_5\text{NH}_2)$	$\text{C}_6\text{H}_5\text{NH}_2$	$\Gamma^-$	I
Electronic energy	-7207.622 32	-7207.493 34	-287.462 97	-7207.499 67	-287.410 96	-6919.960 56	-6919.8380
Zero-point correction	0.116 531			0.117 367	0.116 400		
BSSE	0.002 882			0.001 190			
Calculated energy (eV)		VDE=3.51		EA=3.31			EA=3.33
Observed energy (eV)		VDE=3.59		EA=3.50			EA=3.059 <sup>a</sup>
$ \mu $ (D)		5.30	1.78	4.80	1.18 <sup>b</sup>		

<sup>a</sup>Measured dipole  $|\mu|=1.13\pm 0.02$  D (Ref. 31).

<sup>b</sup>Reference 52.

in this nonequilibrium geometry is large,  $\mu=5.30$  D, pointing from the I atom towards aniline. At the present level of theory, the nascent neutral complex formed by photodetachment is found to be 0.17 eV less stable than the equilibrium neutral complex. The bond dissociation energies of these weakly bonded species are not determined reliably at the current level of theory.

## RESULTS

Results from PPC measurements on  $\Gamma^-(\text{C}_6\text{H}_5\text{NH}_2)$  at photon energies between 3.60 and 4.82 eV are now presented. First, the photoelectron images and spectra are presented and the direct and autodetachment signals are identified and characterized. Then, the dissociation dynamics of the neutral clusters correlated with the autodeattached electrons are differentiated from those correlated with the direct photodetachment processes.

### Photoelectron images and spectra

The photoelectron images and electron kinetic energy spectra resulting from PPC measurements on  $\Gamma^-(\text{C}_6\text{H}_5\text{NH}_2)$  are shown in Fig. 2, plotted on the electron binding energy scale,  $eBE=E_{hv}-eKE$ . Data acquired at 4.82 eV are shown in row (a), 4.00 eV in row (b), 3.76 eV in row (c), and 3.60 eV in row (d). These images and spectra include photoelectrons correlated with *both* bound  $\text{I}(\text{C}_6\text{H}_5\text{NH}_2)$  clusters and the dissociated neutral  $\text{I}+\text{C}_6\text{H}_5\text{NH}_2$  fragments, and also show both the  $v_z$ -sliced  $N(eBE)$  and  $P(eBE)$  spectra as the solid and dashed curves, respectively. The images in Figs. 2(a)–2(c) exhibit both anisotropic and isotropic features. The image in Fig. 2(d), recorded at the lowest photon energy of 3.60 eV, consists only of an isotropic spot of detected electrons. The anisotropic features at the largest radii in each distribution correspond to direct photodetachment from the  $\Gamma^-$  chromophore and have a maximum perpendicular to the laser  $E$  vector, consistent with the  $\sin^2\theta$  photoelectron angular distribution expected for photodetachment of an electron from a  $p$ -like orbital on the solvated  $\Gamma^-$ , as previously discussed for the 4.82 eV data in Ref. 7, where both the ground

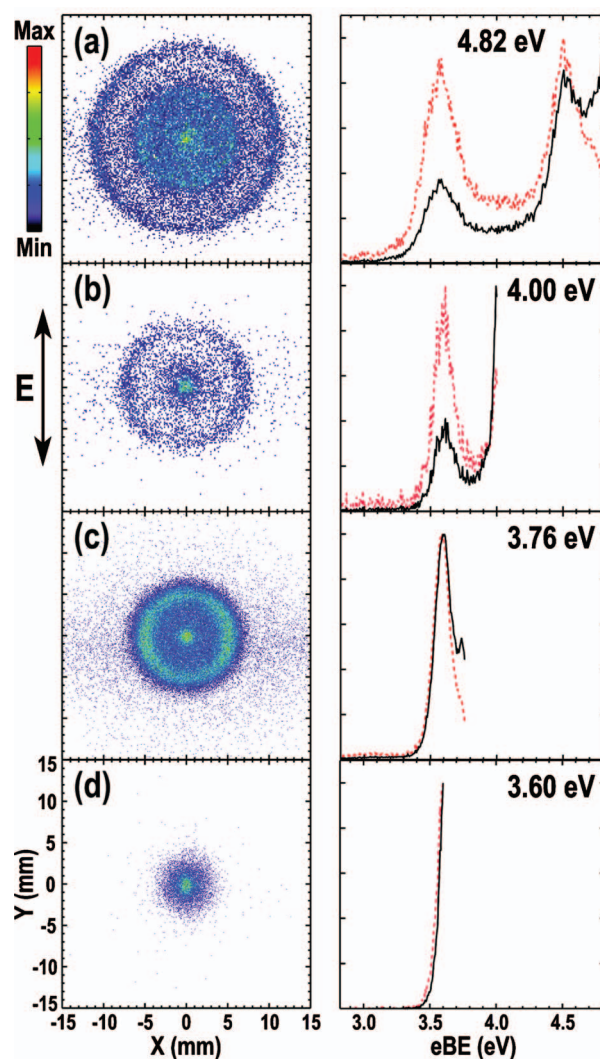


FIG. 2. (Color) Photoelectron images and electron binding energy spectra resulting from (a) 4.82 eV, (b) 4.00 eV, (c) 3.76 eV, and (d) 3.60 eV photodetachments of  $\Gamma^-(\text{C}_6\text{H}_5\text{NH}_2)$ . The electric vector of the laser is parallel to the  $y$  axis in all of the images. The dashed curves are the  $P(eBE)$  spectra and the solid curves are  $v_z$ -sliced  $N(eBE)$  spectra. The electrons included in these images and spectra are correlated with both dissociating and bound neutral clusters.

and excited spin-orbit states of the iodine atom,  $I(^2P_{3/2})$  and  $I(^2P_{1/2})$ , are produced. The isotropic spots present in each of the images are independent of the photon energy and are consistent with the production of low energy electrons by autodetachment.

Examining the data at lower photon energies in more detail, the 4.00 eV  $P(eBE)$  spectrum in Fig. 2(b) reveals a resolved autodetachment feature in addition to a peak correlated with the production of  $I(^2P_{3/2})$ . This is the only  $P(eBE)$  spectrum in which the autodetachment feature is observed as a clearly resolved feature. This photon energy is in between the transitions associated with production of  $I(^2P_{3/2})$  and  $I(^2P_{1/2})$ , showing that the autodetachment feature does not depend on a significant direct photodetachment transition yielding near-threshold photoelectrons.

The results at 3.76 eV are shown in Fig. 2(c). These data were obtained with the lowest photon energy that continues to access nearly the entire envelope of transitions associated with direct photodetachment yielding  $I(^2P_{3/2})$ . Since the eKE resolution increases with decreasing eKE, this spectrum is used to most accurately quantify the VDE of the anionic cluster. The peak in this spectrum yields a VDE =  $3.59 \pm 0.04$  eV for  $I^-(C_6H_5NH_2)$ , representing the energy necessary to remove the excess electron in a vertical, Franck-Condon, process. Assuming the shift observed in the eBE of this complex relative to  $I^-$  is due only to stabilization of the anionic complex, a stabilization energy of 0.53 eV is found for  $I^-(C_6H_5NH_2)$  cluster formation, consistent with the heat of formation reported from negative ion chemical ionization spectrometry measurements.<sup>7,10</sup> As with the spectrum recorded at 4.82 eV, the  $v_z$ -sliced  $N(eBE)$  spectrum clearly shows the central isotropic feature observed in the image as a narrow peak at  $eBE = 3.74 \pm 0.03$  eV, corresponding to electrons detached with very little kinetic energy.

The isotropic spots observed at the centers of each of the images change little with photon energy, consistent with a wavelength-independent autodetachment process yielding electrons with low eKEs (0.0–0.2 eV). In the spectrum recorded at the lowest photon energy (3.60 eV) in Fig. 2(d), only a single spot is observed, probably including both direct and autodetached photoelectrons. The  $P(eBE)$  spectrum shown in Fig. 2(d) extends  $\sim 0.2$  eV below the 3.60 eV photon energy. This near-threshold spectrum yields the best number for the adiabatic electron affinity, EA =  $3.50 \pm 0.10$  eV. The error bars are large owing to an uncertainty in the actual threshold resulting from thermal broadening and spectral congestion in the photodetachment process.

### Photoelectron-photofragment coincidence spectra

The measurement of both photoelectron and photofragment kinetic energies in coincidence is conveniently presented in a PPC spectrum,  $N(E_T, eKE)$ . The  $N(E_T, eKE)$  spectrum at 3.76 eV is shown in Fig. 3, with eKE for photoelectrons correlated with dissociating neutral clusters on the vertical axis and  $E_T$  for the momentum-matched neutrals on the horizontal axis. The corresponding one-dimensional  $P(eKE)$  and  $N(E_T)$  spectra are obtained by integrating the

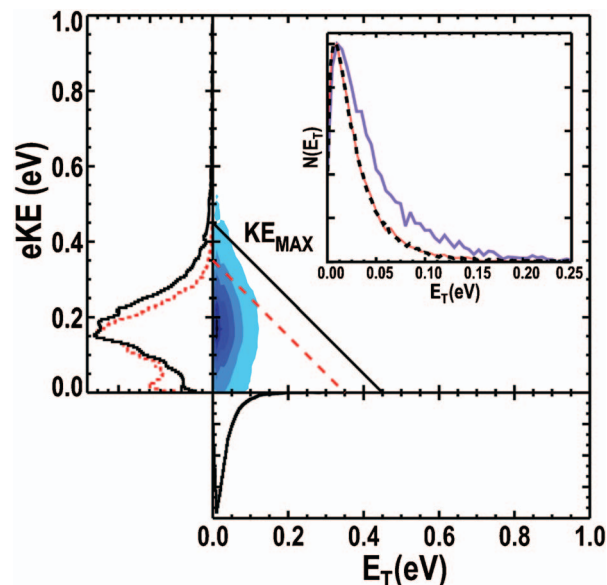


FIG. 3. (Color) Photoelectron-photofragment kinetic energy correlation spectra,  $N(E_T, eKE)$ , for the  $E_{h\nu} = 3.76$  eV DPD of  $I^-(C_6H_5NH_2)$ . Both  $N(eKE)$  and  $P(eKE)$  spectra in coincidence with the fragments are plotted as the dashed and solid curves, respectively, along the y axis. The photofragment translational energy release spectrum,  $N(E_T)$ , is plotted along the x axis. The inset spectra are the electronic-state-dependent  $N(E_T)$  spectra recorded at  $E_{h\nu} = 3.76$  and 4.82 eV. The solid curves result from  $I(^2P_{1/2}) + C_6H_5NH_2$  (larger  $E_T$ ) and  $I(^2P_{3/2}) + C_6H_5NH_2$  at 4.82 eV and the dashed curve results from  $I(^2P_{3/2}) + C_6H_5NH_2$  at 3.76 eV.

coincidence spectrum over the complementary variable, and are shown as the projections along the axes. The  $N(E_T, eKE)$  spectrum reveals the partitioning of the available kinetic energy between the photodetached electron and the neutral fragments. Conservation of energy constrains the energies of the three fragments (photoelectron and two momentum-matched fragments) to lie within the equilateral triangle defined by the horizontal and vertical axes and the maximum kinetic energy carried away by the three bodies,  $KE_{max}$ . The value of  $KE_{max}$  is empirically determined from a  $N(E_T, eKE)$  spectrum from the 5% nominal false-coincidence contour, and represents a measure of the energy required for DPD of the cluster anion. In this system the partitioning of energy favors the photoelectron and the limited eKE resolution results in an underestimation of the anion bond dissociation energy as previously discussed.<sup>7</sup> The  $v_z$ -sliced  $N(eKE)$  spectrum coincident with  $I + C_6H_5NH_2$  photofragments is included in Fig. 3 as the dashed spectrum along the vertical axis, but the events included in the  $N(E_T, eKE)$  spectrum include all photoelectrons correlated with dissociated neutral clusters. The prominent near-zero eKE feature in the dashed-line  $N(eKE)$  spectrum shows that the neutral clusters correlated with autodetached electrons dissociate.

The  $N(E_T, eKE)$  spectrum in Fig. 3 allows further investigation of the electronic-state-dependent half-collision dynamics previously observed at 4.82 eV (Ref. 7) that showed that the  $E_T$  of the neutral products,  $I + C_6H_5NH_2$ , depends on the final spin-orbit state of the I atom. The state-dependent  $N(E_T)$  spectra measured at 4.82 eV are shown as the solid curves in the inset spectra in Fig. 3. The  $N(E_T)$  spectrum for DPD at 3.76 eV is shown in the inset as the dashed curve.

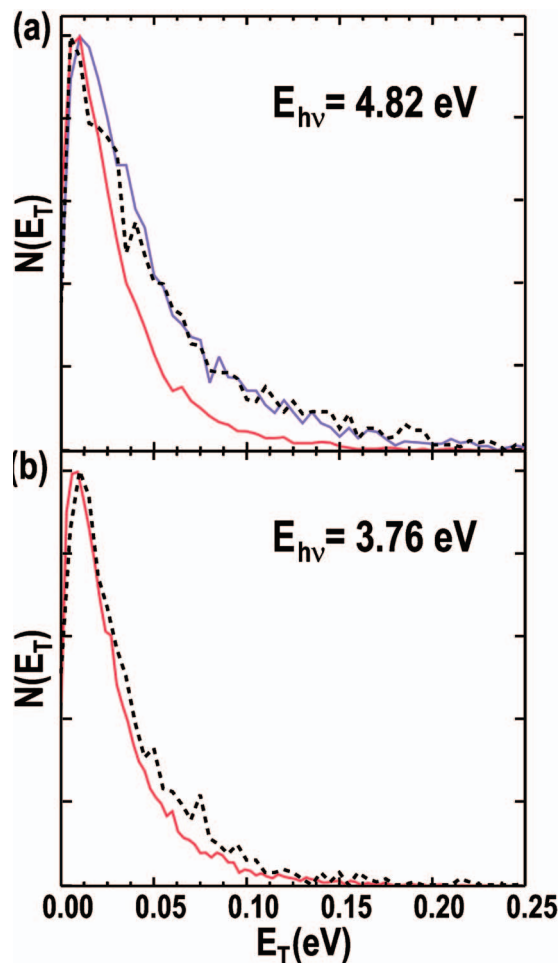


FIG. 4. (Color) Photofragment translational energy spectra,  $N(E_T)$ , from photodetachment of  $\text{I}^-(\text{C}_6\text{H}_5\text{NH}_2)$  at 4.82 eV in panel (a) and at 3.76 eV in panel (b). The  $N(E_T)$  spectra show the energy distribution for neutrals in coincidence with autodetached electrons as dashed curves and neutrals in coincidence with direct DPD as solid curves. In frame (a), the higher energy solid curve corresponds to  $\text{I}^2(\text{P}_{1/2}) + \text{C}_6\text{H}_5\text{NH}_2$  and the lower energy solid curve to  $\text{I}^2(\text{P}_{3/2}) + \text{C}_6\text{H}_5\text{NH}_2$ .

This photon energy only accesses the  $\text{I}^2(\text{P}_{3/2})$  product state, so the dissociation dynamics should match those previously found at 4.82 eV for a Franck-Condon DPD process. As expected, the two spectra match, with an average  $\langle E_T \rangle = 0.030 \pm 0.003$  eV consistent with the previous measurements at 4.82 eV.

#### Autodetachment-photofragment correlation

The  $N(E_T)$  spectra for neutrals correlated with autodetached electrons are compared with  $N(E_T)$  spectra correlated with direct DPD photoelectrons in Figs. 4(a) and 4(b) for measurements at 4.82 and 3.76 eV, respectively. These  $N(E_T)$  spectra are generated by integrating the  $N(E_T, \text{eKE})$  spectra over the appropriate eKE ranges. In the 4.82 eV spectrum, the  $N(E_T)$  spectrum for autodetachment includes all  $\text{eKE} \leq 0.2$  eV, with all  $\text{eKE} > 0.2$  eV constituting the  $N(E_T)$  spectrum for direct photodetachment. At 3.76 eV, autodetachment includes all photoelectrons with  $\text{eKE} \leq 0.05$  eV, and all higher eKEs constitute the direct photodetachment  $N(E_T)$  spectrum. The 4.82 eV spectrum can also be resolved with respect to the spin-orbit states of the I atom

product. The direct DPD  $N(E_T)$  spectrum at 4.82 eV (Ref. 7) is resolved into contributions for  $\text{I}^2(\text{P}_{1/2})$  in the range  $0.2 \leq \text{eKE} \leq 0.55$  eV and  $\text{I}^2(\text{P}_{3/2})$  in the range  $0.85 \leq \text{eKE} \leq 1.6$  eV.

The  $N(E_T)$  spectra show that the dissociation dynamics of clusters correlated with autodetached electrons match the  $N(E_T)$  spectra for direct photodetachment to the I atom spin-orbit state closest to threshold at a given photon energy. The neutrals correlated with autodetached electrons at 4.82 eV have a greater  $N(E_T)$ , consistent with that observed for direct DPD to  $\text{I}^2(\text{P}_{1/2})$  at that photon energy. The neutrals correlated with autodetached electrons have  $\langle E_T \rangle = 0.056 \pm 0.005$  eV, while those correlated with direct photodetachment to  $\text{I}^2(\text{P}_{1/2})$  and  $\text{I}^2(\text{P}_{3/2})$  have  $\langle E_T \rangle = 0.049 \pm 0.004$  eV and  $\langle E_T \rangle = 0.031 \pm 0.003$  eV, respectively. At the lower photon energy of 3.76 eV, it is found that neutrals correlated with autodetached electrons have  $\langle E_T \rangle = 0.035 \pm 0.003$  eV, in good agreement with those correlated with direct photodetachment to  $\text{I}^2(\text{P}_{3/2})$  products:  $\langle E_T \rangle = 0.030 \pm 0.003$  eV.

As illustrated above, the near-zero eKE features associated with autodetachment are accentuated by viewing the  $v_z$ -sliced  $N(\text{eBE})$  spectra. The  $N(\text{eBE})$  spectra at 4.82 and 3.76 eV correlated with neutral clusters that dissociate are shown as the solid curves in Figs. 5(a) and 5(b), respectively. The autodetachment features are identified as the peaks at  $\text{eBE} = E_{h\nu}$  ( $\text{eKE} \cong 0$  eV). The dashed spectra in these figures are the  $N(\text{eBE})$  spectra correlated with stable neutral  $\text{I}(\text{C}_6\text{H}_5\text{NH}_2)$  clusters only, generated through the spherical gating procedure previously described.<sup>7</sup> The most significant difference between these spectra is the lack of the autodetachment feature in the spectra correlated with stable neutral clusters.

#### DISCUSSION

The experiments presented here probe the wavelength-dependent photodetachment dynamics of  $\text{I}^-(\text{C}_6\text{H}_5\text{NH}_2)$  at photon energies from 3.60 to 4.82 eV. The photodetached neutral clusters were monitored in coincidence with the photoelectrons and the dissociation dynamics of unstable clusters resulting from both direct DPD and autodetachment were characterized. This discussion will focus on the nature of the autodetachment process that occurs in  $\text{I}^-(\text{C}_6\text{H}_5\text{NH}_2)$  and the associated DPD dynamics. The fundamental observation made is that an autodetachment process occurs over the entire range of photon energies. Autodetachment is correlated with dissociation products only, and the dissociation dynamics observed are nearly identical with the lowest energy direct DPD process at a given photon energy.

As discussed in the Introduction, an excited state of the cluster anion accessible over a wide range of photon energies must be responsible for the autodetachment process in  $\text{I}^-(\text{C}_6\text{H}_5\text{NH}_2)$ . Direct photodetachment of the I<sup>-</sup> chromophore is the dominant process in this cluster, and as previously shown,<sup>7</sup> the dissociation dynamics of the  $\text{I}(\text{C}_6\text{H}_5\text{NH}_2)$  neutral clusters exhibit a dependence on the final spin-orbit state of the I atom product for those clusters that dissociate. The autodetachment process is correlated

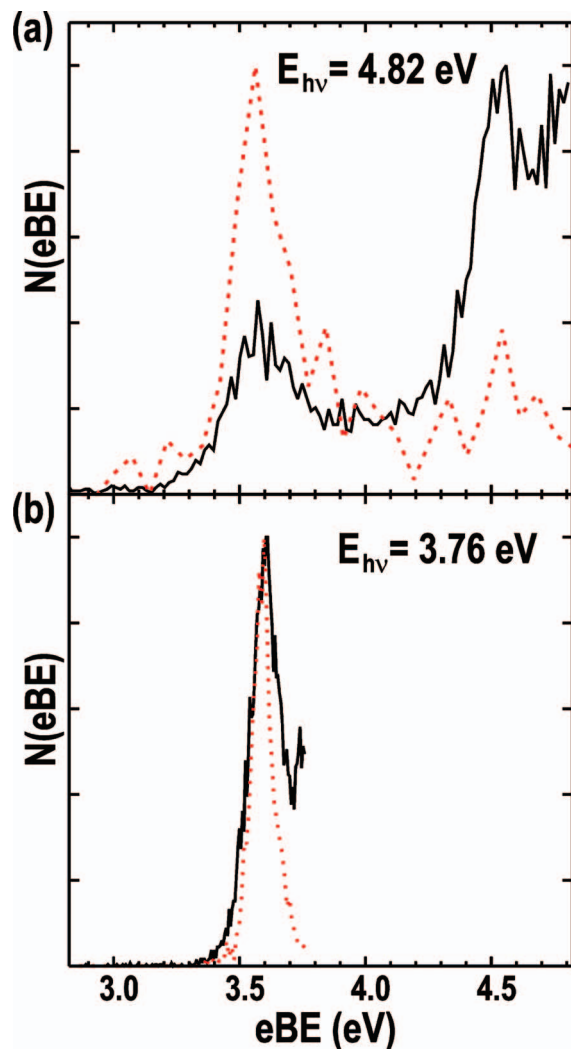


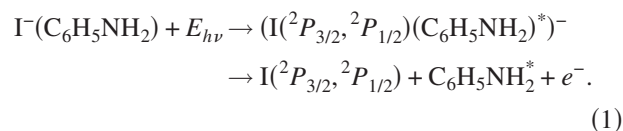
FIG. 5. (Color) Photoelectron  $N(eBE)$  spectra from photodetachment of  $\Gamma^-(C_6H_5NH_2)$  at 4.82 eV in panel (a) and at 3.76 eV in panel (b). The  $N(eBE)$  spectra show electrons in coincidence with stable neutral clusters as the dashed curves and with  $I+C_6H_5NH_2$  photofragments as the solid curves.

only with dissociation products, not stable clusters. The strongest evidence that the autodetachment feature is coupled with the direct photodetachment of the  $\Gamma^-$  moiety is that the dissociation dynamics of clusters correlated with photodetachment match those for the direct process [yielding  $I(^2P_{3/2})$  or  $I(^2P_{1/2})$ ] closest to threshold at a given photon energy. This argues strongly against autodetachment arising from photoexcitation of the aniline moiety, followed by electronic or vibrational autodetachment of the electron localized on the I atom. This is in spite of the fact that the strong  $S_0 \rightarrow S_1$  transition in isolated aniline at 4.22 eV (Ref. 46) is likely to be accessible at a number of the photon energies studied here.

The most likely explanation for the autodetachment feature involves a competition between direct photodetachment and a CTTS process leading to temporary localization of the excess electron in an excited state of the complex or the aniline moiety. As discussed in the Introduction, both types of processes have been previously observed. Charge transfer into the low-lying  $a_2(\pi_1^*)$  orbital of aniline observed in electron transmission measurements<sup>32</sup> is certainly energetically

accessible at the highest photon energies used here, and may in fact be accessible over the entire photon energy range as the presence of the I atom in the nascent neutral complex may stabilize this valence excited state. Detailed excited-state calculations on the neutral cluster are beyond the scope of the present work, but the DFT calculations performed suggest instead that the large dipole (5.3 D) of the nascent neutral cluster is likely to support a transient dipole-bound state that decays by autodetachment as the cluster dissociates.

The following mechanism is proposed for autodetachment of a transient dipole-bound excited state competing with direct photodetachment:



This mechanism involves absorption of a photon by the anionic complex, initiating the direct photodetachment process. The nascent neutral  $I(C_6H_5NH_2)$  cluster, born in the equilibrium geometry of the anionic complex, has a substantially enhanced dipole moment that interacts with the incipient continuum electrons, capturing a fraction of the lower energy electrons into a diffuse, transient dipole-bound excited state of the distorted iodine-aniline cluster. Upon photodetachment, the electrostatic interaction binding  $\Gamma^-$  and  $C_6H_5NH_2$  is lost and on the time scale of nuclear motion the cluster begins relaxing toward the neutral cluster equilibrium geometry and  $\sim 95\%$  of all neutral clusters subsequently dissociate.<sup>7</sup> Capture of some photoelectrons by the transient dipole in the distorted neutral cluster has no impact on the evolving dissociation dynamics of the complex as a result of the minimal interaction between the diffuse excess electron and the  $I(C_6H_5NH_2)^*$  core, resulting in no effect on the spin-orbit state dependence of the dissociation dynamics seen in direct photodetachment. As the dissociation proceeds and aniline relaxes to the equilibrium structure, the transient dipole decreases and the dipole-bound electron is ejected with very little kinetic energy, yielding the observed wavelength-independent autodetachment signal and an internally excited aniline molecule.

This proposed autodetachment mechanism is similar to that invoked in a series of investigations by Johnson and co-workers of the microscopic precursor to the CTTS reaction in iodide-acetone and iodide-acetonitrile clusters. In those studies, photoexcitation below the detachment threshold transferred the excess electron from the halide to the molecular solvent via capture by the dipole field of the solvent.<sup>12,17,24</sup> Both acetone and acetonitrile have sufficient dipole moments to support a long-lived dipole-bound molecular anion, and the stability of this anion is responsible for the CTTS band observed below the detachment threshold. In the studies presented here, the photon energy is always greater than the minimum energy required for direct photodetachment of the  $\Gamma^-$  chromophore, but the photodetachment dynamics are suggestive of a similar CTTS reaction followed by autodetachment from an excited, dipole-bound state of  $\Gamma^-(C_6H_5NH_2)$ . The primary difference between the systems studied by Johnson and co-workers and the one presented

here is that both acetone and acetonitrile have sufficiently strong dipole moments to capture and retain an electron to form the dipole-bound ground states of those molecular anions<sup>45,46</sup> ( $\mu=2.88$  D for acetone<sup>47</sup> and 3.92 D for acetonitrile<sup>31</sup>), without the need for halide-induced geometrical distortion. Mabbs *et al.* have studied the binary  $\Gamma(\text{CH}_3\text{CN})$  and  $\Gamma(\text{CH}_3\text{I})$  clusters using photoelectron imaging at 267 nm recently and seen no evidence for autodetachment processes occurring in these species.<sup>9</sup> In the case of  $\Gamma(\text{CH}_3\text{CN})$ , this is likely to be a result of the strength of the dipole field of  $\text{CH}_3\text{CN}$  supporting retention of the extra electron. In the case of  $\Gamma(\text{CH}_3\text{I})$ , as noted in the Introduction, Cyr *et al.* observed the occurrence of intracluster dissociative attachment in this species,<sup>33</sup> so if some of the electrons are captured by the  $\text{CH}_3\text{I}$  moiety, production of  $\text{I}^-$  at some time after the 100 fs pulse laser used by Mabbs *et al.* may occur.

As discussed in the Introduction, there have been previous studies of the CTTS process in iodide-water clusters, including time-resolved photoelectron spectroscopy measurements of the  $\Gamma(\text{H}_2\text{O})_4$  and  $\Gamma(\text{D}_2\text{O})_4$  clusters<sup>26,27</sup> and most recently studies of the dissociation dynamics of the  $\text{I}(\text{H}_2\text{O})_n$ ,  $n=2,5$ , clusters photoexcited to the CTTS band.<sup>30</sup> These systems begin to truly probe CTTS processes in that the solvent shell can reorganize and more effectively respond to photoexcitation and charge transfer than the aniline molecule. An interesting aspect of the recent study by Szpunar *et al.*<sup>30</sup> is that they concluded that the likely mechanism for DPD of  $\Gamma(\text{H}_2\text{O})_n$ ,  $n=2-5$ , involved autodetachment followed by dissociation. The results seen here for  $\Gamma(\text{C}_6\text{H}_5\text{NH}_2)$ , in which the autodetached electrons are correlated with dissociation products bearing the dynamical signature of the distinct I atom spin-orbit channels, suggest that dissociation occurs prior or simultaneously with autodetachment.

A remarkable aspect of the results reported here is that wavelength-independent autodetachment is observed over a photon energy range of 1.2 eV. There is an example of autodetachment observed over an even wider photon energy range in the studies of the photodetachment dynamics of  $(\text{OCS})_2^-$  by Surber and Sanov from 1.55 to 4.64 eV.<sup>48,49</sup> The homomolecular dimer anion  $(\text{OCS})_2^-$  is known to exhibit isomeric forms and is also likely to have a rich excited-state spectrum owing to the possibility for symmetric charge transfer. Ionic photodissociation is known from previous work to be important in this system as well.<sup>50</sup> In  $(\text{OCS})_2^-$ , these observations were attributed to either autodetachment from an electronically excited state of the dimer anion or autodetachment from the unstable  $\text{OCS}^-$  photodissociation product. In the present case of  $\text{I}(\text{C}_6\text{H}_5\text{NH}_2)^-$ , charge transfer to a valence excited state of aniline would be analogous to the proposed mechanism for the  $(\text{OCS})_2^-$  dimer anion, but the evidence that the autodetachment dissociation dynamics match those of the I atom spin-orbit channel closest to threshold argues that in the present work autodetachment originates from interaction of the nascent neutral cluster dipole with the direct photodetachment process.

## CONCLUSIONS

An experimental study of the direct photodetachment and autodetachment dynamics of the iodide-aniline cluster,  $\Gamma(\text{C}_6\text{H}_5\text{NH}_2)$ , at four photon energies from 3.60 to 4.82 eV has been presented. PPC spectroscopy was used to investigate the half-collision dynamics of the nascent neutral clusters correlated with the two distinct electron detachment processes. The wavelength-independent autodetachment process is proposed to originate from formation of a temporary dipole-bound anionic state stabilized by the large dipole of the nascent neutral  $\text{I}(\text{C}_6\text{H}_5\text{NH}_2)$  cluster configured in the geometry of the anion. Dissociation of the neutral cluster destroys the large dipole as the aniline fragment relaxes to its equilibrium structure, liberating a low energy electron. The neutral fragments correlated with the autodetached electrons were observed to follow the direct DPD dynamics of the I atom product spin-orbit state closest to threshold at each photon energy. This observation is consistent with perturbation of the direct photodetachment process by the large dipole of the cluster as the origin of the two-step sequential mechanism leading to autodetachment.

## ACKNOWLEDGMENTS

Support for this research was provided by the National Science Foundation (Grant No. CHE-0136195). One of the authors (M.B.) acknowledges support from MIUR and for his stay at UCSD from the Joint Research Center of the European Commission under the Sixth Framework Program's Marie Curie Transfer of Knowledge fellowship (Contract No. MTKD-CT-2004-509761).

- <sup>1</sup>W. H. Robertson and M. A. Johnson, *Annu. Rev. Phys. Chem.* **54**, 173 (2003).
- <sup>2</sup>L. Oudejans and R. E. Miller, *Annu. Rev. Phys. Chem.* **52**, 607 (2001).
- <sup>3</sup>A. W. Castleman and K. H. Bowen, *J. Phys. Chem.* **100**, 12911 (1996).
- <sup>4</sup>A. Sanov and W. C. Lineberger, *Phys. Chem. Chem. Phys.* **6**, 2018 (2004).
- <sup>5</sup>K. LeBarbu, J. Schiedt, R. Weinkauff, E. W. Schlag, J. M. Nilles, S. J. Xu, O. C. Thomas, and K. H. Bowen, *J. Chem. Phys.* **116**, 9663 (2002).
- <sup>6</sup>Z. M. Loh, R. L. Wilson, D. A. Wild, E. J. Bieske, and A. Zehnacker, *J. Chem. Phys.* **119**, 9559 (2003).
- <sup>7</sup>M. S. Bowen, M. Becucci, and R. E. Continetti, *J. Phys. Chem. A* **109**, 11781 (2005).
- <sup>8</sup>D. W. Arnold, S. E. Bradforth, E. H. Kim, and D. M. Neumark, *J. Chem. Phys.* **102**, 3510 (1995).
- <sup>9</sup>R. Mabbs, E. Surber, and A. Sanov, *J. Chem. Phys.* **122**, 0543081 (2005).
- <sup>10</sup>G. W. Caldwell, J. A. Masucci, and M. G. Ikononou, *Org. Mass Spectrom.* **24**, 8 (1989).
- <sup>11</sup>D. W. Arnold, S. E. Bradforth, E. H. Kim, and D. M. Neumark, *J. Chem. Phys.* **97**, 9468 (1992).
- <sup>12</sup>C. E. H. Dessent, C. G. Bailey, and M. A. Johnson, *J. Chem. Phys.* **102**, 2006 (1995).
- <sup>13</sup>C. Bassmann, U. Boesl, D. Yang, G. Drechsler, and E. W. Schlag, *Int. J. Mass Spectrom. Ion Process.* **159**, 153 (1996).
- <sup>14</sup>C. Frischkorn, M. T. Zanni, A. V. Davis, and D. M. Neumark, *Faraday Discuss.* **115**, 49 (2000).
- <sup>15</sup>R. S. Berry, in *Advances in Electronics and Electron Physics*, edited by L. Marton and C. Marton (Academic, New York, 1980), Vol. 51, pp. 137-182.
- <sup>16</sup>U. Hefter, R. D. Mead, P. A. Schulz, and W. C. Lineberger, *Phys. Rev. A* **28**, 1429 (1983).
- <sup>17</sup>C. E. H. Dessent, C. G. Bailey, and M. A. Johnson, *J. Chem. Phys.* **102**, 6335 (1995).
- <sup>18</sup>W. R. Garrett, *Phys. Rev. A* **3**, 961 (1971).

- <sup>19</sup>W. R. Garrett, J. Chem. Phys. **73**, 5721 (1980).
- <sup>20</sup>C. Desfrancois, H. Abdoul-Carime, N. Khelifa, and J. P. Schermann, Phys. Rev. Lett. **73**, 2436 (1994).
- <sup>21</sup>W. R. Garrett, J. Chem. Phys. **77**, 3666 (1982).
- <sup>22</sup>S. F. Wong and G. J. Schulz, Phys. Rev. Lett. **33**, 134 (1974).
- <sup>23</sup>K. Rohr and F. Linder, J. Phys. B **9**, 2521 (1976).
- <sup>24</sup>D. Serxner, C. E. H. Dessent, and M. A. Johnson, J. Chem. Phys. **105**, 7231 (1996).
- <sup>25</sup>K. D. Jordan and F. Wang, Annu. Rev. Phys. Chem. **54**, 367 (2003).
- <sup>26</sup>L. Lehr, M. T. Zanni, C. Frischkorn, R. Weinkauff, and D. M. Neumark, Science **284**, 635 (1999).
- <sup>27</sup>A. V. Davis, M. T. Zanni, C. Frischkorn, and D. M. Neumark, J. Electron Spectrosc. Relat. Phenom. **108**, 203 (2000).
- <sup>28</sup>S. S. Xantheas and J. T. H. Dunning, J. Chem. Phys. **99**, 8774 (1993).
- <sup>29</sup>J. E. Combariza, N. R. Kestner, and J. Jortner, J. Chem. Phys. **100**, 2851 (1994).
- <sup>30</sup>D. E. Szpunar, K. E. Kautzman, A. E. Faulhaber, and D. M. Neumark, J. Chem. Phys. **124**, 054318 (2006).
- <sup>31</sup>*CRC Handbook of Chemistry and Physics*, 86th ed. (Taylor and Francis, Boca Raton, FL, 2005).
- <sup>32</sup>K. D. Jordan, J. A. Michejda, and P. D. Burrow, J. Am. Chem. Soc. **98**, 7189 (1976).
- <sup>33</sup>D. M. Cyr, C. G. Bailey, D. Serxner, M. G. Scarton, and M. A. Johnson, J. Chem. Phys. **101**, 10507 (1994).
- <sup>34</sup>R. E. Continetti, Int. Rev. Phys. Chem. **17**, 227 (1998).
- <sup>35</sup>L. S. Alconcel, H. J. Deyerl, M. DeClue, and R. E. Continetti, J. Am. Chem. Soc. **123**, 3125 (2001).
- <sup>36</sup>J. A. Davies, J. E. LeClaire, R. E. Continetti, and C. C. Hayden, J. Chem. Phys. **111**, 1 (1999).
- <sup>37</sup>M. S. Bowen and R. E. Continetti, J. Phys. Chem. A **108**, 7827 (2004).
- <sup>38</sup>M. J. Frisch, G. W. Trucks, H. B. Schlegel *et al.*, GAUSSIAN 2003.
- <sup>39</sup>A. Sanov, J. Faeder, R. Parson, and W. C. Lineberger, Chem. Phys. Lett. **313**, 812 (1999).
- <sup>40</sup>M. Kowal, R. W. Gora, and S. Roszak, J. Chem. Phys. **115**, 9260 (2001).
- <sup>41</sup>N. Godbout, D. R. Salahub, J. Andzelm, and E. Wimmer, Can. J. Chem. **70**, 560 (1992).
- <sup>42</sup>D. E. Woon and T. H. Dunning, J. Chem. Phys. **98**, 1358 (1993).
- <sup>43</sup>S. F. Bois and F. Bernardi, Mol. Phys. **19**, 553 (1970).
- <sup>44</sup>W. E. Sinclair and D. W. Pratt, J. Chem. Phys. **105**, 7942 (1996).
- <sup>45</sup>J. A. Stockdale, F. J. Davis, R. N. Compton, and C. E. Klots, J. Chem. Phys. **60**, 4279 (1974).
- <sup>46</sup>C. G. Bailey, C. E. H. Dessent, and M. A. Johnson, J. Chem. Phys. **104**, 6976 (1996).
- <sup>47</sup>R. D. Nelson, D. R. Lide, and A. A. Maryott, *Selected Values of Electric Dipole Moments for Molecules in the Gas Phase*, Natl. Bur. Stand. Ref. Data Ser., No. 10, Natl. Bur. Stand. (US GPO, Washington, D.C., 1967).
- <sup>48</sup>E. Surber and A. Sanov, Phys. Rev. Lett. **90**, 0930011 (2003).
- <sup>49</sup>E. Surber and A. Sanov, J. Chem. Phys. **118**, 9192 (2003).
- <sup>50</sup>A. Sanov, S. Nandi, K. D. Jordan, and W. C. Lineberger, J. Chem. Phys. **109**, 1264 (1998).
- <sup>51</sup>P. Csaszar and P. Pulay, J. Mol. Struct. **114**, 31 (1984).
- <sup>52</sup>C. E. Moore, *Atomic Energy Levels*, Natl. Bur. Stand. Circ. No. 467 (US GPO, Washington, D.C., 1958).